

Interfacial modification mechanism of nanocellulose as a compatibilizer for immiscible binary poly(vinyl alcohol)/poly(ethylene oxide) blends

Cheng Yong,¹ Changtong Mei ,¹ Mingjie Guan,¹ Qinglin Wu,² Xiuxuan Sun,² Bing Xu,¹ Ke Wang¹

¹College of Materials Science and Engineering, Nanjing Forestry University, Nanjing, Jiangsu 210037, China

²School of Renewable Natural Resources, Louisiana State University, Baton Rouge, Louisiana 70803

Correspondence to: C. Mei (E-mail: mei@njfu.edu.cn)

ABSTRACT: We undertook this study to understand reinforcement mechanism of short cellulose nanocrystals (CNCs) and long cellulose nanofibrils (CNFs) as compatibility agents for improving the interfacial miscibility of poly(vinyl alcohol) (PVA) and poly(ethylene oxide) (PEO) blends. The effects of the two cellulose nanofibers on the morphological, mechanical, and thermal properties of the polymer blends were compared systematically. The light transparency, scanning electron microscopy, and Fourier transform infrared results show that nanocellulose between PVA and PEO eliminated the negative effects generated by the immiscible interface through increased hydrogen bonding. Thermogravimetric analysis and differential scanning calorimetry results show that crystalline region reorganization around the interface facilitated the shift of the polymer blends from multiple phases to a homogeneous phase. According to the Halpin-Kardos and Quali models, we assumed that the potential for repairing the immiscible interface would have a larger effect than the potential of reinforcement. At the same concentration, polymer blends with CNCs showed greater light transparency, strength, modulus, and crystal structure than with those with CNFs. © 2017 Wiley Periodicals, Inc. *J. Appl. Polym. Sci.* 2017, 135, 45896.

KEYWORDS: differential scanning calorimetry; nanoparticles, nanowires, and nanocrystals; surfaces and interfaces; theory and modeling

Received 19 May 2017; accepted 17 September 2017

DOI: 10.1002/app.45896

INTRODUCTION

Polymer blending is an effective method for manufacturing advanced materials with excellent properties, as the blending of multiple polymer components creates a synergistic effect and yields a comprehensive overall performance with desired chemical and mechanical properties.^{1,2} However, most binary blends are immiscible because of the unmatched enthalpies of their polymer blends. A separated interface and weak interfacial bonding greatly restricts the combinations of binary polymers, as the interfacial properties are closely related to the adhesion and tension at the interface that quantifies compatibility.³ Previous studies have indicated that the miscibility of two polymer blends is dependent not only on each component's properties but also strongly on the interfacial morphology and interfacial adhesion.⁴ Moreover, most polymer pairs are thermodynamically incompatible because of small rejections between the chains of the macromolecular monomers; this can result in increased entropy by polymer blending.⁵ For this reason, the industrial applications of immiscible polymer blends may be limited largely because of these imperfectly bonded interfaces. In general, a suitable compatibilizer is introduced to interdiffuse into polymer blends to optimize their interfacial morphology and improve their interfacial adhesion.²

Both poly(vinyl alcohol) (PVA) and poly(ethylene oxide) (PEO) are industrial polymers with hydrophilic, biocompatible, and nontoxic properties, and their blending can yield significant practical utility.^{5,6} It is naturally taken for granted that the C—O—C groups of PEO would form hydrogen bonds with the neighboring —OH groups from PVA. However, many studies have discovered an obvious liquid–liquid separated interface in the PVA–PEO blend system. Mishra and Rao⁷ reported that the hydrogen adhesion between PVA and PEO may be negligible, according to the results of Fourier transform infrared (FTIR) and NMR spectroscopy. Lai and Liao⁸ tested the glass-transition temperature of a PVA–PEO blend, showing two glass-transition temperature values matching those of PVA and PEO; this showed the system to be immiscible. Sawatari and Kondo⁹ demonstrated the immiscibility of PVA–PEO films on the basis of small-angle light scattering, wide-angle X-ray diffraction, and FTIR spectroscopy, and they also concluded that only the primary hydroxyl groups of cellulose interacted with the oxygen of PEO. PVA, with only secondary hydroxyl groups, could not interact with the skeletal oxygen of PEO. Therefore, some studies have focused on choosing an appropriate compatibilizer to modify the PVA–PEO interface. An environmental and biocompatible cellulose derivative could be used as a compatibilizer to

form partly miscible blends with the syntheses of PVA and PEO at the molecular scale.^{10,11}

As representative cellulose derivatives, both cellulose nanocrystals (CNCs) and cellulose nanofibrils (CNFs) have been incorporated as desired reinforcing agents into PVA matrixes or PEO matrixes with hydrogen bonding.^{12–14} CNCs are usually extracted from fibers after the complete dissolution of the non-crystalline regions, whereas CNFs are obtained from mechanical shearing, which leads to a high degree of fibrillation.^{14,15} CNCs are rodlike, short, crystalline cellulosic nanoparticles, whereas CNFs are flexible, semicrystalline fibers with relatively long fiber networks compared to CNCs. Numerous studies have reported that CNFs, with their small diameters and longer lengths, showed better mechanical enhancement abilities for PVA or PEO, whereas CNCs, with their smaller lengths, served as better nucleation agents than CNFs because longer fiber entanglements restricted the growth of crystallites.¹⁴ Despite most previous studies having illustrated good reinforcing effects for both CNCs and CNFs in a pure polymer or binary polymers, a side-by-side comparison of their interfacial immiscibility modification and reinforcing abilities in terms of nanofiber diameter, morphology, crystallization, and mechanical properties in polymer blending has not been attempted.

In this study, various ratios of CNCs and CNFs were used to improve the interfacial miscibility of the PVA–PEO blends as compatibilizers to better understand the contributions of the enhanced interface to the properties of PVA–PEO nanocomposites. The experimental tensile properties were compared with theoretical predictions from the Halpin–Kardos and Quali models combined with different cellulose structures. We expected this work to cement the role of different forms of nanocellulose as interfacial compatibilizers or as reinforcing agents in PVA–PEO blends and to determine which role was dominant. Finally, a schematic diagram based on the interfacial miscibility transformation of the PVA–PEO blends by the addition of nanocellulose was used to demonstrate and predict the notable enhancement of their mechanical and thermal properties. The models from this study showed that nanocellulose facilitated a dynamic shift from multiple phases to a homogeneous phase by the method of breaking the crystalline regions. The extraordinary results from this study show great potential for medical and industrial applications and will provide practical guidance for the application of nanocellulose as an interfacial compatibilizer in designing batteries, phase-change materials, storage materials, and self-healing materials.^{11,12,16}

EXPERIMENTAL

Materials

PVA (average weight-average molecular weight = 88,000–97,000, 98–99% hydrolyzed) and PEO (average weight-average molecular weight = 100,000) were purchased from Alfa Aesar as matrixes for the binary polymer blends. The CNCs were extracted from wood pulp, and their detailed preparation method was described in our previous article,¹⁷ whereas the CNFs were of microfibrillated cellulose origin (solid content = 25%) and were purchased from Intelligent Chemicals Pty, Ltd. (China). Briefly, the CNCs were prepared with 64 wt %

sulfuric acid hydrolysis, several centrifugation cycles, and high-pressure homogenization. The length and diameter of the CNCs were 163.0 ± 20.9 and 15.6 ± 2.6 nm, respectively.¹⁷ The CNFs were prepared through repeated high-pressure homogenization. The average length and diameter were 1030 ± 334 and 20 ± 14 nm, respectively.¹⁴

Sample Preparation

The PVA–PEO nanocomposite films reinforced by CNCs or CNFs were prepared by solution casting. PVA was first dissolved in deionized water by stirring at 80 °C to form a homogeneous solution with the concentration of 5 wt %, and then, PEO with the same concentration was added to maintain the desired proportion of 70/30 with a total concentration of 5 wt %. Different ratios of CNC or CNF suspensions were poured into the PVA–PEO blends to make compounds containing 0, 3, or 6 wt % CNCs or CNFs (depending on the polymer blend weight). The specific formulations of the PVA, PEO, PVA–PEO (70/30) blend, PVA–PEO (70/30) blend with 3% CNCs or 6% CNCs, and PVA–PEO (70/30) blend with 3% CNFs or 6% CNFs were designated as PVA, PEO, PE3, PEC3, PEC6, PEF3, and PEF6, respectively. After magnetic stirring for 6 h, some blend solutions were applied to the miscibility study, whereas some blend solutions were poured into Petri dishes, dried at room temperature for 7 days, and then placed in a vacuum oven at 30 °C for another 7 days to finally yield nanocomposite films without water.

Characterization Methods

Miscibility Study. The light transmittance of the single solution and polymer mixture solutions with various ratios of CNCs or CNFs after magnetic stirring for 6 h was tested with a UV–visible spectrophotometer (Evolution 600 PC). All of the samples were scanned from 300 to 900 nm at a scanning speed of 240 nm/min.

Interfacial Morphology. The interfacial morphologies of the polymer blend films were investigated with a scanning electron microscope (S-340, Hitachi, Japan) at a 10 kV accelerating voltage. All of the films were cooled in liquid nitrogen for 10 min and then immediately fractured. The cryofractured interfaces of the composites were sputter-coated with a thin layer of gold before viewing.

FTIR Testing. FTIR measurements of the pure polymer and polymer blend films with CNCs or CNFs were performed with a Bruker FTIR analyzer (Tensor-27, Germany) in transmittance mode (4000 – 500 cm^{-1}) at room temperature. The transmission mode combined with 32 scans with a resolution of 4 cm^{-1} under attenuated total reflectance mode was used for each sample.

Tensile Properties. The tensile modulus and strength of the polymer blend films were studied with the AR2000EX rheometer (TA Instruments) with a solid fixture. The dimensions of the rectangular sample cuttings from the blend films were 15 mm (length) \times 3 mm (width) \times 0.2 mm (thickness). The gauge length between the two grips was set as 10 mm for this test, and the speed of testing was 10 $\mu\text{m/s}$. The tensile stress and

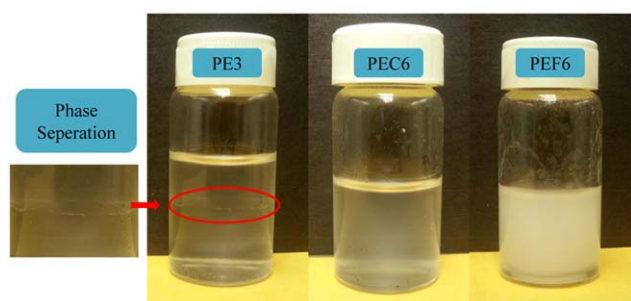


Figure 1. Solutions of polymer blends and their blends with 6 wt % CNCs or CNFs. [Color figure can be viewed at wileyonlinelibrary.com]

elongation at break were calculated from the recorded force and displacement.

Thermogravimetric Analysis (TGA). The thermal stabilities of the polymer blend films were measured with a thermogravimetric analyzer (Q50, TA Instruments). Each sample of approximately 5 mg was heated from 30 to 600 °C at a heating rate of 10 °C/min. Each experiment was performed under a nitrogen flow of 40 mL/min and was repeated three times.

Melting and Crystallization Behaviors. A differential scanning calorimeter (200 F3, Netzsch, Germany) was used to study the melting and crystallization behaviors of the polymer blend films. All samples were first heated from 35 to 240 °C at a heating rate of 20 °C/min and held there for 10 min to erase the residual thermal stress. Subsequently, all of the samples were cooled to 0 °C at the same rate and kept there for 10 min. Then, the samples were reheated from 0 to 240 °C at the same rate to investigate the melting behavior without any thermal history. All of these procedures were conducted under nitrogen purge gas at a rate of 40 mL/min.

The crystallinity (X_c) of the samples was obtained by the following expression:

$$X_c = \frac{\Delta H_m / \phi}{\Delta H_m^*} \times 100\% \quad (1)$$

where ΔH_m is the melting enthalpy obtained from the differential scanning calorimetry (DSC) curves, ΔH_m^* is the melting enthalpy of the 100% crystalline polymer, and ϕ is the weight fraction of each polymer in the composites. The ΔH_m^* values reported in previous work^{8,11} were 156 J/g for PVA and 197 J/g for PEO.

RESULTS AND DISCUSSION

Miscibility Properties

Figure 1 shows a visual comparison of the phase separation and phase uniformization in the binary PVA–PEO blends and their nanocomposites with 6 wt % CNCs or CNFs after magnetic stirring for 6 h and standing for 30 s. The separated interface in the initial transparent solution clearly showed the intrinsic incompatibility of PVA and PEO, as discussed in previous literature.⁹ However, the addition of CNCs or CNFs as a compatibility agent significantly increased the possibility of interfacial miscibility in the PVA and PEO components through hydrogen adhesion, as shown in Figure 2. This hydrogen adhesion with

the ether groups of PEO and the hydroxyl groups of PVA made the solution miscible and, thus, eliminated the interfacial separation. The solution was more transparent for the 6 wt % CNC reinforced polymer blends than for the CNF blends. The longer fibers of the CNFs tangled with each other, exhibited a disordered structure, and prohibited light transmittance;¹⁸ thereby, this provided a good example of the importance of choosing appropriate nanoparticles for optical applications.

As depicted in Figure 3(a), both the pure PVA and PEO solutions were highly transparent, whereas the transmittance value at 900 nm of the binary polymer blends decreased from approximately 80% in the PEO solution to 20% in the blends; this supported the interfacial immiscibility. As shown in Figure 3(b), the addition of CNCs or CNFs clearly reduced the transmittance of the polymer blend solution because of the possible space hindrance effect of the solid nanoparticles. However, the increase in CNCs from 3 to 6% improved the transmittance of the blend solution from 7.2 to 12.3% at 900 nm; this made the blend solution more transparent, whereas the addition of CNFs may have led to a counterproductive effect. These effects may have been due to competition between the hydrogen bonding from cellulose repairing the immiscible interface and the solid nanoparticles, which hindered the light transparency.¹⁵ Clearly, the short and directed CNCs with less entanglement exhibited a better restorative effect as compatibility agents in the PVA and PEO blends.

Morphology

Fractured interfaces of the PVA and PEO blends and their nanocomposites with 6 wt % CNCs or CNFs were observed in scanning electron microscopy images shown in Figure 4. As depicted in Figure 4(A,a), a faintly visible transition interfacial region appeared; this indicated an immiscible and very thin interpenetrating interface between PVA and PEO. PVA and PEO with different properties showed different shrinkage coefficients under the same cooling conditions; this led to a raised edge between them. An inclined crack and many pores also existed near the centerline of the interface; there were more and larger pores when they were closer to the centerline of the interface.

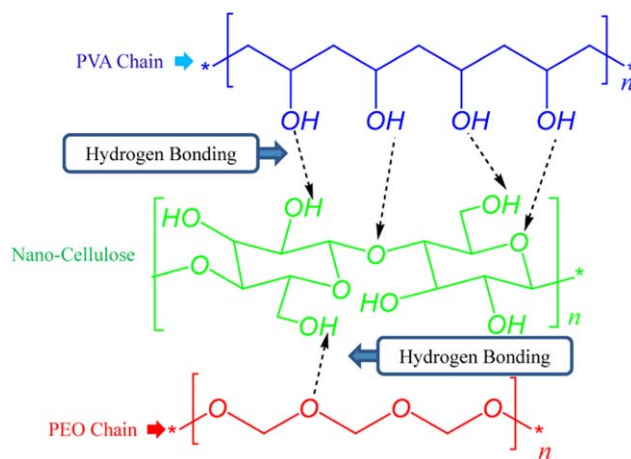


Figure 2. Schematic illustration model of the PVA and PEO interactions with nanocellulose. [Color figure can be viewed at wileyonlinelibrary.com]

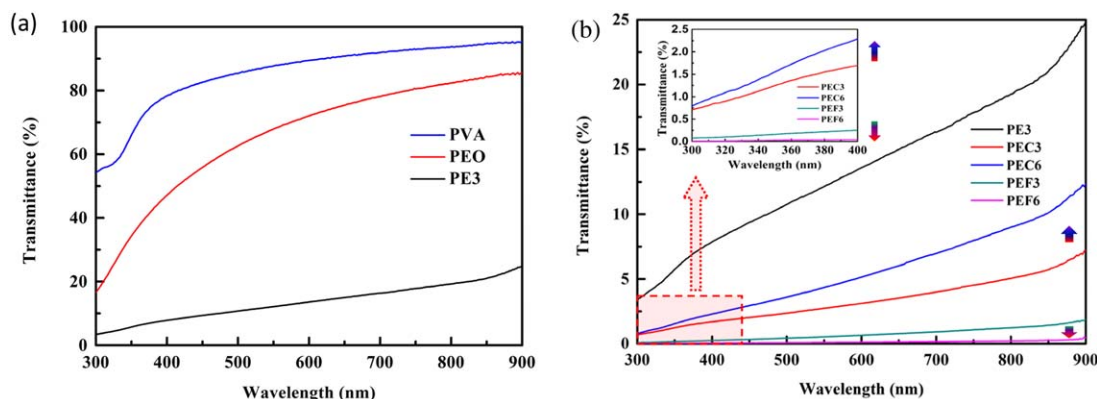


Figure 3. Solution transmittance of the (a) pure polymers and polymer blends and (b) polymer blends and their blends with different concentrations of CNCs or CNFs. [Color figure can be viewed at wileyonlinelibrary.com]

This phenomenon may be further effective evidence of the immiscible interface, which could be explained by the pores and cracks resulting from air trapped within the film during water evaporation, despite the degassing of the suspension, and interfacial shrinkage caused by liquid nitrogen cooling. PVA and PEO have different properties; this led to different degrees of discordance under the changed conditions and resulted in the appearance of pores and cracks.

In the nanocomposites shown in Figure 4(B,b,C,c), no obvious transition interfacial region existed, and the number and size of the pores decreased significantly; this indicated improved compatibility between PVA and PEO because of the interactions provided by the nanocellulose hydroxyl groups. Compared with the smooth fractured interface of the polymer blends, the interfaces of the nanocomposites with 6 wt % CNCs or CNFs were not uniform, and the CNF nanocomposites exhibited a raised lamellar structure, whereas the CNC nanocomposites showed a slightly raised, compact regiment. Similar phenomena were reported in previous literature,¹⁹ as directed long fibers may

demonstrate their reinforcing effect and greatly restrict the matrix when the composite is forced and fractured, as shown by the lamellar interfacial morphology depicted in Figure 4(c). It may be easier for longer fibers to form a big proportion of visibly pulled-out nanofibers and fibrils entangling on the interface because of their larger aspect ratios.¹⁴

FTIR Analysis

FTIR spectroscopy was used to evaluate the hydrogen-bonding interactions between the CNCs (or CNFs) and the PVA–PEO matrix, as shown in Figure 5. As depicted in Figure 5(a), the FTIR spectra of the pure polymers and their blend films were consistent with those in previous reports.^{7,20} In the spectra, above 2000 cm^{-1} , the broad peak at 3284 cm^{-1} and the vibrational band at 2886 cm^{-1} corresponded to $-\text{OH}$ groups and $-\text{CH}$ stretching, respectively. In the spectra below 2000 cm^{-1} , the most important peaks were the $\text{C}=\text{O}$ stretching vibrations at 1558, the $\text{C}-\text{O}-\text{C}$ stretching vibrations at approximately 1144–1058 cm^{-1} from the nonhydrolyzed vinyl acetate groups of PVA and the ether groups of PEO, and the $-\text{CH}_2$ rocking

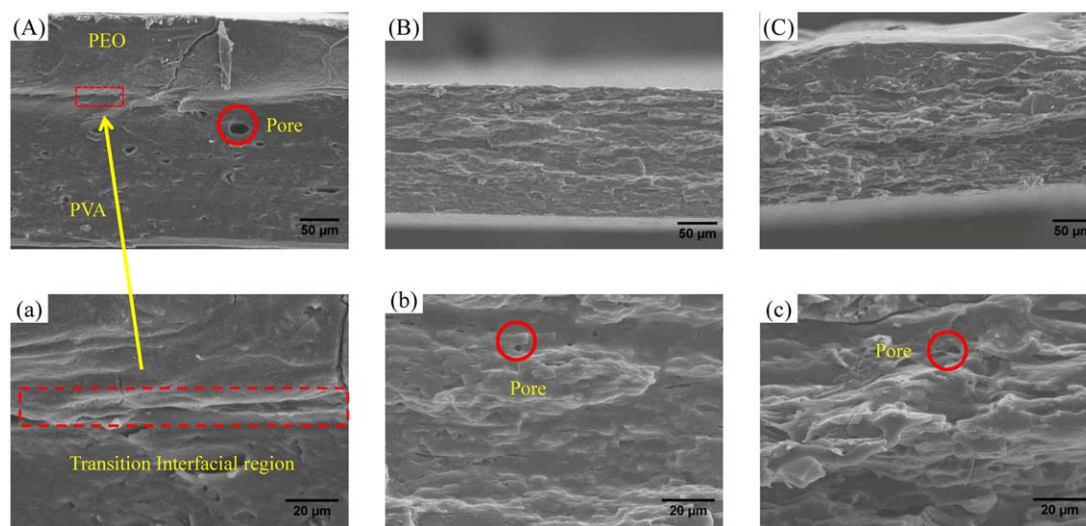


Figure 4. Fractured interfacial morphologies of the (A) polymer blends at 300 \times and (a) polymer blends at 1000 \times and their nanocomposites with (B) 6 wt % CNCs at 300 \times , (b) 6 wt % CNCs at 1000 \times , (C) 6 wt % CNFs at 300 \times , and (c) 6 wt % CNFs at 1000 \times . [Color figure can be viewed at wileyonlinelibrary.com]

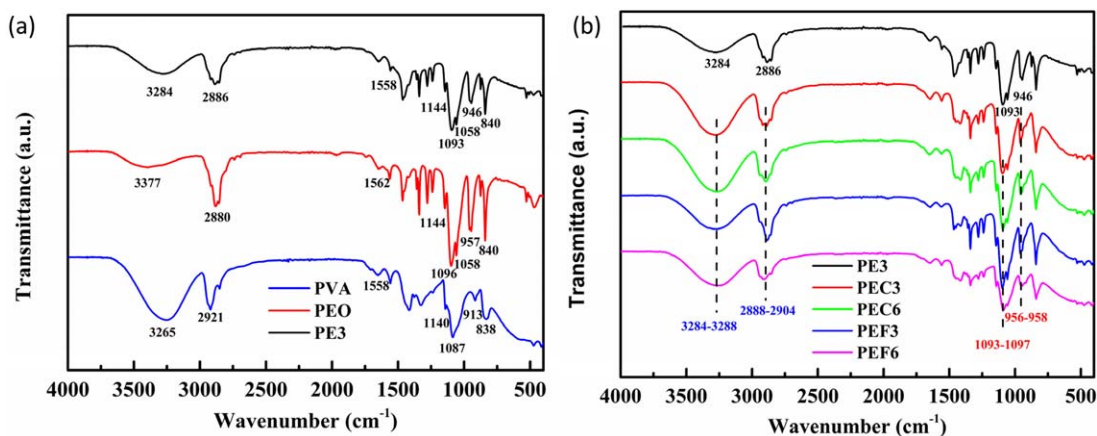


Figure 5. FTIR curves of the (a) pure polymers and polymer blends and (b) polymer blends and their nanocomposites with different concentrations of CNCs or CNFs. [Color figure can be viewed at wileyonlinelibrary.com]

vibrations¹¹ at 946 and 840 cm^{-1} . In the blend film spectrum, no new characteristic peak of binary polymer blends was found, and the peak values of the polymer blends were neutralized and shifted toward different values in the pure polymers; this indicated that no significant intermolecular interactions between PVA and PEO existed.

The FTIR spectra in Figure 5(b) show the intensities and values of the characteristic peaks of the nanocomposites with 3 and 6 wt % CNCs or CNFs. The intensities of the bands at 3284–3288 and 2888–2904 cm^{-1} , which were due to the —OH stretching vibrations and —CH stretching from nanocellulose¹⁷ and the PVA–PEO matrix, respectively, were strengthened and shifted toward higher frequencies with increased nanocellulose concentration. As is clear from the FTIR results, the CNCs exhibited better compatibility than the CNFs for PVA and PEO interfacial miscibility. This may have been partly due to interfibrillar hydrogen bonding between the nanocellulose and the PVA–PEO matrix; this led to the self-healing of the immiscible interface. The stretching bands for C—O—C (1093–1097 and 956–958 cm^{-1}) shifted to high values; this may have been due to a crystallinity change.^{21,22} This was further evidence of a modified interface and is subsequently discussed in detail.

Mechanical Properties

It is well known that the nanosize effect and high modulus of nanocellulose are perfect for polymer reinforcement.¹³ The typical stress–strain curves for nanocellulose-reinforced polymer blends are depicted in Figure 5(a). The detailed corresponding data is listed in Table I. As shown in Figure 5(a), the PVA and

PEO blends exhibited a long plastic yielding behavior and were fractured after the strain reached the yielding region. After the addition of the CNCs or CNFs to the polymers, no obvious yielding region was observed; this indicated the presence of possible brittle fracture. Most notably, the addition of CNCs or CNFs contributed to great increases in the tensile modulus and strength.

When the concentration of the CNCs or CNFs increased, the tensile modulus and strength increased, as shown in Table I. The optimal values appeared at 6% for both the CNCs and CNFs. As shown in Table I and Figure 6(a), the nanocomposites containing 6 wt % CNCs or CNFs showed Young's modulus values of 7743 and 6872 MPa, tensile strengths of 234 and 210 MPa, and strains at failure of 14.6 and 13.7%, respectively. The strain results decreased by probably four-fold for the CNC- and CNF-reinforced polymer blends compared with the neat polymer blends. These increases in the modulus and strength were attributed to the high CNC and CNF mechanical properties and their interactions with PVA and PEO through hydrogen bonding. For ductility, the incorporation of both the CNCs and CNFs caused a decrease in the elongation at break because of the stress concentration of the nanoparticles in the relatively ductile PVA and PEO blends under tensile loadings.²³ It is worth noting that the polymer blends with the CNCs exhibited better mechanical properties than those with the CNFs; as shown in Table I, as the concentration increased from 0 to 3 wt % CNCs and CNFs, the modulus increased by 38.5 and 19.9%, respectively, and the strength increased by 17.8 and 12.7%, respectively.

Table I. Tensile Properties of the Polymer Blends and Their Nanocomposite Films with Different CNC or CNF Contents

Filler	Content	Young's modulus (MPa)	Yield strength (MPa)	Strain at failure (%)
	0	1634 ± 168	91.7 ± 8.2	60.1 ± 7.8
CNCs	3	6292 ± 741	162.9 ± 20.2	14.1 ± 3.7
	6	7743 ± 510	234.1 ± 38.3	14.6 ± 2.9
CNFs	3	3250 ± 143	116.9 ± 9.0	13.6 ± 3.8
	6	6872 ± 960	210.1 ± 35.8	13.7 ± 1.5

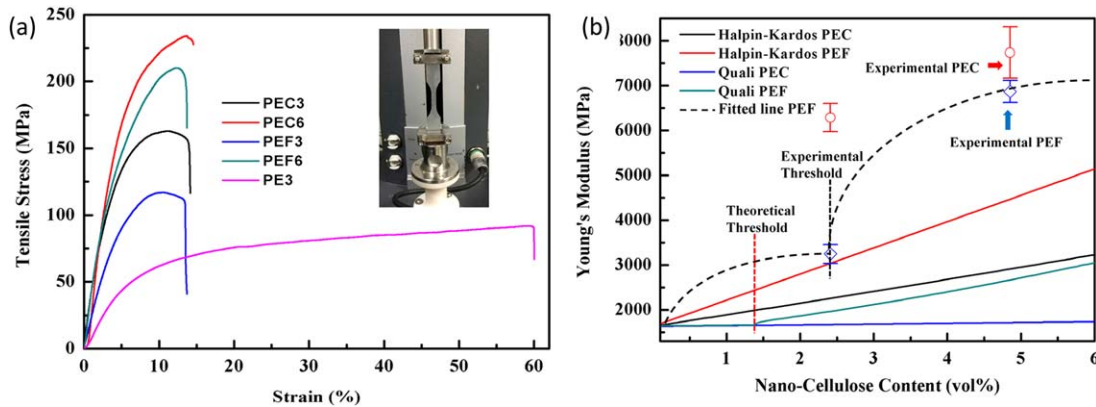


Figure 6. (a) Typical stress–strain curves in tension for the polymer blends with different contents of CNCs or CNFs and (b) experimental values of Young's modulus versus the model predictions. [Color figure can be viewed at wileyonlinelibrary.com]

Combined with the scanning electron microscopy results, these results were incredibly important because it is assumed that added CNCs or CNFs should be capable of connecting with hydrophilic polymers such as PVA or PEO and constraining the polymer molecular movement, thereby decreasing the elongation.²⁴ However, some of the mechanical reinforcement was also assumed to originate from the improved miscible interface between PVA and PEO, whereas the interfacial debonding could not ensure stress transfer sufficiently in mechanical property reinforcement.

To compare the interfacial repairing potential and reinforcing potential of the CNCs and CNFs in the PVA–PEO blend matrixes, the Halpin-Kardos and Quali models were applied to simulate the modulus values of the nanocomposite films, and the simulation values were compared with the experiment results. The Halpin-Kardos semiempirical model was suggested to speculate the modulus of oriented short-fiber composites and has been applied in nanocellulose composites.^{14,25} The Young's modulus can be calculated as follows:

$$E_{\parallel} = E_m \frac{1 + \eta_{\parallel} \zeta \phi_f}{1 - \eta_{\parallel} \phi_f} \quad (2)$$

$$E_{\perp} = E_m \frac{1 + 2\eta_{\perp} \phi_f}{1 - \eta_{\perp} \phi_f} \quad (3)$$

where

$$\eta_{\parallel} = \frac{\frac{E_f}{E_m} - 1}{\frac{E_f}{E_m} + \zeta} \quad (4)$$

$$\eta_{\perp} = \frac{\frac{E_f}{E_m} - 1}{\frac{E_f}{E_m} + 2} \quad (5)$$

where E_{\parallel} and E_{\perp} are the longitudinal and transverse Young's moduli of the matrix, respectively; ϕ_f is the filler volume fraction; E_m is the modulus of the matrix; E_f is the modulus of the filler; and ζ is a dimensional parameter related to the filler length/diameter ratio and can be obtained from the length (L) and diameter (w). The relation $\zeta = 2L/w$ is applied to relatively short fibers, such as CNCs, whereas $\zeta = (0.5L/w)^{1.8}$ was suggested by Van Es for relatively long fillers.²⁶ The modulus of a

nondirectional composite (E_c) can be measured according to the following equation:²³

$$E_c = 0.184E_{\parallel} + 0.816E_{\perp} \quad (6)$$

The following values were obtained directly from or calculated from the experiments used in the theoretical calculation: E_m was 1634 MPa, and E_f of the CNCs (CNFs) was 145,000 MPa (79,000 MPa).^{27,28} The length of the CNCs (CNFs) was 159 nm (1030 nm), and their diameter was 15 nm (20 nm) according to our previous article¹⁷ and related literature.¹⁴ The volume fraction of the CNCs (CNFs) was calculated by the following expression:

$$\phi_f = \frac{\frac{w_f}{\rho_f}}{\left[\frac{w_f}{\rho_f} + \frac{(1-w_f)}{\rho_m} \right]} \quad (7)$$

where w_f is the mass fraction of the CNCs (CNFs) at 3 or 6 wt %; ρ_f is the density of the CNCs (CNFs) and was estimated to be 1.59 g/cm³; and ρ_m is the density of PVA–PEO blends calculated from the density of PVA and PEO and was estimated to be 1.25 g/cm³.

The Quali model was extended on the basis of the series-parallel model of Takayanagi.^{29,30} This model takes into account the percolation concept, which is dependent on the experimental data at temperatures higher than the transition temperature of the matrix polymer.^{22,31} Accordingly, this model can be written as follows:

$$E_c = \frac{(1-2\psi + \psi\phi_f)E_m E_f + (1-\phi_f)\psi E_f^2}{(1-\phi_f)E_f + (\phi_f - \psi)E_m} \quad (8)$$

where ψ is the percolating volume fraction of filler network and can be expressed as follows:

$$\psi = 0 \quad \phi_f \leq \phi_c \quad (9)$$

$$\psi = \phi_f \left(\frac{\phi_f - \phi_{fc}}{1 - \phi_{fc}} \right)^b \quad \phi_f > \phi_c \quad (10)$$

where b is the critical percolation exponent and is estimated to be 0.4 for a three-dimensional network^{29,30} and ϕ_c is the critical volume fraction (percolation threshold) as per the following expression:

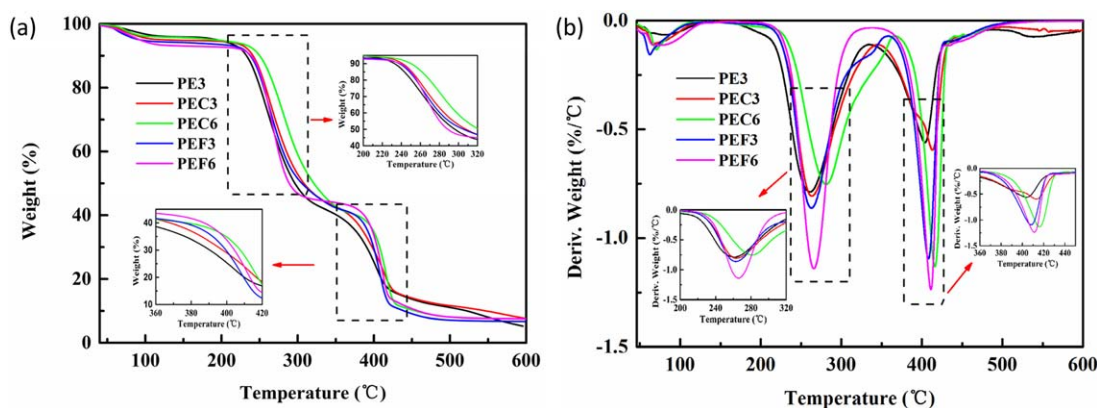


Figure 7. (a) TGA and (b) DTG curves for the polymer blends and their nanocomposites with different concentrations of CNCs or CNFs. [Color figure can be viewed at wileyonlinelibrary.com]

$$\varphi_c = \frac{0.7}{(L/w)} \quad (11)$$

The experimental data of the polymer blend nanocomposites along with the theoretical data from these two models are shown in Figure 5(b). Unexpectedly, neither of these classic models gave a precise prediction within the range of nanocellulose concentrations. The Halpin-Kardos model results were relatively close to the experimental results, whereas the percolation model seemed to capture the modulus jumping basically by coincidence. The experimental modulus of the nanocomposite with CNCs was higher than that of the nanocomposite with CNFs at the same content; this was contrary to the results of some published articles.¹⁴ Also, the modulus jumping of the nanocomposite with CNCs was before 3 wt % for the Quail model, but this phenomenon was supposed to occur after a content of 6 wt %, ²⁵ whereas the modulus jumping of the nanocomposite with CNFs seemed to be captured at 3 wt %. As shown by the fitted line PEF in Figure 5(b), the big deviation between the theoretical data and the experimental data was due to the immiscible interfacial compatibility and the changes in the size of nanocellulose in the evaporation process of the PVA–PEO solution.

The Halpin-Kardos model is an empirical model dependent on a self-consistent theory where fibers have a good dispersion in and adhesion to the matrix; it does not account for interactions between the fibers. However, the Quail model takes the fiber–fiber interactions into consideration when the volume ratio of fibers exceeds its threshold through the percolating filler phase.

The different prediction results especially emphasize this comparison of filler–filler interactions and filler–matrix interactions at high filler contents. However, these models only regard the fiber as a type of reinforcing particle in one polymer, ignoring their potential to repair the immiscible interface between binary polymers. It is easier for CNFs, with their larger aspect ratio, to entangle and form networks with the matrix through hydrogen adhesion. Conversely, CNCs, with their short aspect ratio, can disperse sufficiently into the matrix; this provides more chances for them to align with the PVA and PEO chains. Because of the weak interface between PVA and PEO, the original modulus of the blend matrix should be underestimated, and the greatly increased modulus comprised many factors, such as the fiber entanglement, interfacial modification, and improved crystallization region (discussed in detail subsequently), not solely mechanical interlocking through hydrogen bonding. Obviously, the polymer blends with CNCs exhibited better mechanical properties than with those with CNFs at the same content because of the priority of interfacial modification. The effect of mechanical interlocking may have been weakened for CNCs and CNFs because of an unstable interface.

Thermal Stability

The dynamic thermogravimetric curves and corresponding derivative thermogravimetry (DTG) curves of the PVA and PEO blends and their nanocomposites with various contents of CNCs or CNFs are shown in Figure 7; the corresponding characteristic data are listed in Table II. As is shown in Figure 7(a),

Table II. TGA and DTG Results for the PVA and PEO Blends and Their Nanocomposites with Different Concentrations of CNCs or CNFs

Filler	Content	Onset degradation temperature (°C)	Stage I		Stage II		Char yield after thermal degradation (%)
			T_{max} (°C)	Maximum weight loss rate (%/min)	T_{max} (°C)	Maximum weight loss rate (%/min)	
	0	232.8	261.1	0.79	403.8	0.56	5.23
CNCs	3	241.3	263.4	0.81	413.0	0.60	7.47
	6	250.1	281.1	0.75	416.1	1.13	7.48
CNFs	3	237.8	263.1	0.86	408.2	1.09	6.67
	6	238.8	266.3	1.14	411.1	1.24	7.50

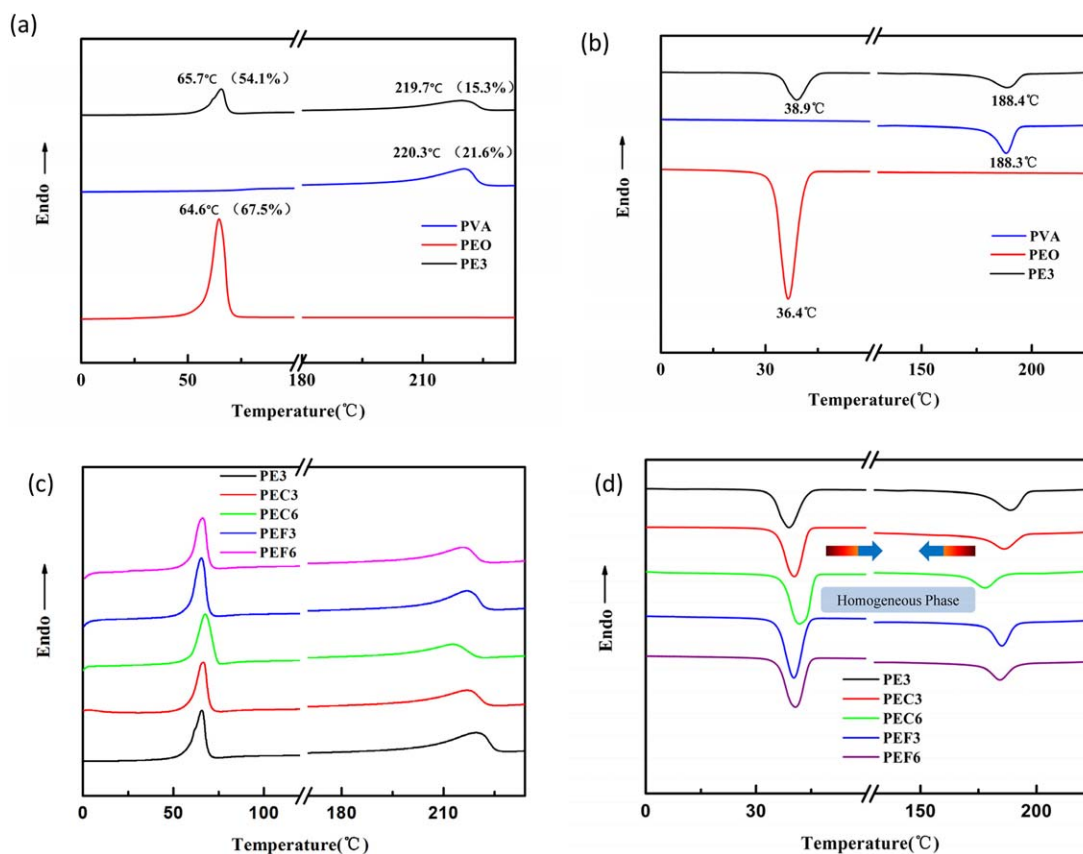


Figure 8. Melting and crystallization behaviors of the (a,b) pure polymers and their blends and (c,d) polymer blends and their nanocomposites with various CNC or CNF contents. [Color figure can be viewed at wileyonlinelibrary.com]

the pure PVA had two stages of decomposition, whereas there was only a single sharp decomposition in the pure PEO. For PVA, the first decomposition region, at approximately 250–370 °C, was due to the degradation of the PVA chain, whereas the second region, at approximately 380–500 °C, was due to the carbonation of the polymer matrix and was followed by a final decomposition of the polymer.^{32,33} PEO exhibited only a single-stage degradation, which occurred at approximately 367–450 °C by the random chain scission of C–O bonds.^{34,35} The TGA and DTG curves of the PVA and PEO blends are presented in ref. ²⁰. The polymer blends exhibited two obvious degradation steps, which were attributed to the coefficient factors of decomposition of PVA and PEO.

Samples containing 6 wt % CNCs exhibited an onset temperature that increased from 232.8 to 250.1 °C, a maximum degradation temperature of the first peak that increased from 261.1 to 281.1 °C, and a maximum degradation temperature of the second peak from 403.8 to 416.1 °C. This similar reinforcement also appeared in the CNF nanocomposites. This phenomenon may be explained by two aspects:

1. The thermal properties of the polymer blends were not degraded by the addition of nanocellulose; however, the nanocellulose interacted with PVA and PEO separately and formed interlocking and entanglements. This improved the thermal stability of the polymer blends.

2. As the original thermal stability of the polymer blends may have been presumed to have decreased after polymer blending, the interfacial compatibilization from nanocellulose may be desired more urgently than the reinforcement from fillers.

We also concluded from the temperature corresponding to the first and the second peak of DTG curves (T_{max}) in Table II that the thermal stability of the polymer blends with CNCs was better than that with CNFs at the same content because of the immiscible interfacial modification. The CNC nanocomposites were assumed to show a much lower temperature at which the maximum mass loss rate occurred due to the sulfate groups from the CNCs during the manufacturing process.^{36,37} The influence of the miscible interface may have been dominant and should be placed ahead of other factors such as reinforcement.

Melting and Crystallization Behaviors

The DSC thermograms of the pure PVA, PEO, and their nanocomposite films with different contents of CNCs or CNFs are shown in Figure 6(a–d), and the related parameters are summarized in Table III. For the melting behaviors shown in Figure 8(a), the peak melting temperature of the polymer blends exhibited two peaks at 65.7 and 219.7 °C. The values were very close to those of PEO and PVA. Additionally, the crystallinities of the polymer blends, which arose from PVA and PEO, suffered a drop to various degrees. A similar phenomenon based

Table III. DSC Results for the PVA and PEO Blends and Their Nanocomposites with Different Concentrations of CNCs or CNFs

Sample	eT_m (°C)	pT_m (°C)	eT_c (°C)	pT_c (°C)	$^e\Delta H_m$ (J/g)	$^p\Delta H_m$ (J/g)	eX_c (%)	pX_c (%)
PE3	65.7	219.7	38.9	188.4	31.98	16.53	54.1	15.3
PEC3	66.4	217.1	40.5	186.0	35.39	13.82	61.7	13.0
PEC6	67.6	212.7	41.2	177.8	32.87	9.76	60.0	9.5
PEF3	65.4	216.7	40.3	185.2	36.56	15.33	63.7	14.9
PEF6	66.1	215.6	40.7	184.1	33.18	13.27	59.5	12.9

eT_m and pT_m , peak melting temperatures of PEO and PVA, respectively; eT_c and pT_c , peak crystallization temperatures of PEO and PVA, respectively; $^e\Delta H_m$ and $^p\Delta H_m$, melt enthalpies of PEO and PVA, respectively; eX_c and pX_c , crystallinities of PEO and PVA, respectively.

on the crystalline behaviors was also found, as shown in Figure 8(b), because of the presence of a separated interface in the polymer blends and a strong signature of interfacial immiscibility. We assumed that an incompatible interface between PVA and PEO may have acted back on the matrixes themselves because of the influence of crystalline region interdiffusion; this led to a possible transcristallization phenomenon.³⁸

The addition of CNCs or CNFs to the blends created remarkable changes in the melting temperatures, as depicted in Figure 6(c). The characteristic melting peak of PEO in the polymer blends shifted toward much higher temperatures with the addition of nanocellulose from 0 to 6 wt %, whereas the peak melting temperature of PVA shifted to much lower temperatures. In addition, the crystallization of the polymer blends as a function of the CNC or CNF concentration generated different trends for PVA and PEO. The crystallization of PEO (for PVA–PEO blends) increased first from 51.4 to 61.7 and 63.7 wt % with 3 wt % nanocellulose followed by decreases to 60.0 and 59.5% with 6 wt % nanocellulose, whereas only a decrease was captured for the crystallization from the PVA region. Similar results were also inferred from the crystallization behavior, as shown in Figure 8(d), where the peak crystallization temperature originating from PEO increased with increasing nanocellulose content, whereas the peak crystallization temperature of the blends for PVA exhibited a downward trend.

Both the peak melting temperature and peak crystallization temperature trended toward the center. We ascribed a structural origin to the obvious increase in the melting temperature of PEO because of the influence of the PVA in the interfacial zone. The addition of CNCs or CNFs induced PVA and PEO away from a crystalline order and may have been responsible for the irregular crystallinities of PVA and PEO. These induced ordered PVA and PEO could be absorbed by the cellulose nanoparticles through linking to the “rigid amorphous phase” concept of Wunderlich.³⁹ The reduced crystalline region restarted crosslinking one by one in favor of hydrogen bonding from cellulose and began to form a dynamic homogeneous phase. The new layers ordered in this manner by entanglement redispersed into the polymer blends and began to break down the old structure and form new layers by cellulose absorption. Cellulose in this blend effectively facilitated the formation of a stable and miscible interface as a compatibilizer. The crystallinity change and interfacial modification were the main reasons for the improved

mechanical properties and shifted functional group positions, as discussed previously (a further detailed discussion is included in the next section). The CNC nanocomposites exhibited a trend toward a relatively homogeneous phase because of the closer peak melting and crystallization temperatures generated from PVA and PEO. The decrease in the crystallinities of the CNC nanocomposites was more significant than that of the CNF nanocomposites. One factor corresponding to the reinforced interfacial miscibility greatly explained this. Because of their small size, the CNCs were able to sufficiently disperse into the matrix to generate more chances to break down the crystalline region of PVA and PEO.²⁶ Nucleation was placed in the secondary position, as the miscibility of the polymer blends exhibited more power toward the overall properties than the strengthening only of a single component.

Mechanism for the Reinforcement Based on Interfacial Modification

A mechanism of improved interfacial immiscibility is schematically illustrated in Figure 9; this shows how nanocellulose was presumed to play a critical role in changing the structures of the PVA and PEO blends. For the neat PVA–PEO blends [Figure 9(a,b)], the crystal region of the interactive interface was compressed by the interdiffusion of PVA and PEO chains. With little significant hydrogen bonding from the nonhydrolyzed vinyl acetate groups of PVA and the ether groups of PEO, this separated interface was immiscible; this resulted in decreased mechanical properties and crystallinity because of discontinuous stress transfer from one polymer to the other and mutual interference in the crystalline region.

With the addition of nanocellulose, as shown in Figure 9(c,d), two factors were introduced for the reinforcement of the overall nanocomposites. (1) Generally, nanocellulose itself had the potential to reinforce hydrophilic polymers because of the strong affinity of PVA and PEO with the reactive cellulose surface. Because of its high specific area, it was easy for nanocellulose to disperse in the matrix with hydroxyl groups; this led to the formation of a rigid network with PVA and PEO and, thereby, assisted in fiber–matrix and fiber–fiber load transfer and facilitated the earlier behavior of the brittle region. (2) An improvement from the high modulus of the fibers is generally appropriate for a single polymer but is of limited effectiveness for binary or ternary blends. As shown in this study, the interfacial miscibility was the predominant factor determining the final

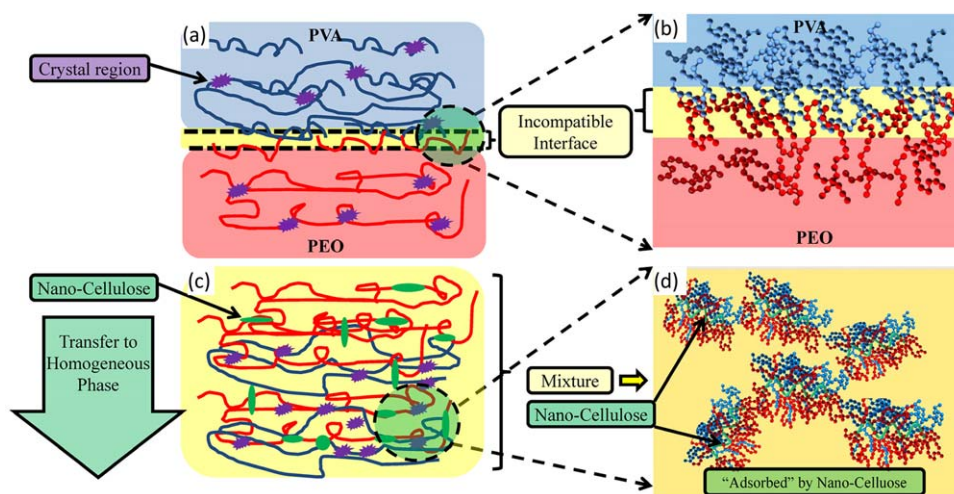


Figure 9. Schematic illustration of the mechanism for improved interfacial miscibility: (a) PVA and PEO blend with a separated interface, (b) high magnification of the immiscible interface between the PVA and PEO chains, (c) relative homogeneous phase of the polymer blends with cellulose, and (d) high magnification of the adsorption for PVA and PEO chains generated by nanocellulose. [Color figure can be viewed at wileyonlinelibrary.com]

properties of the composites rather than any single property from one component. It was assumed that some nanoparticles with nonselective interactions with the polymer blends localized at the polymer–polymer interface when the entropic loss of the nanoparticles upon localization at the interface was compensated for breaking down the crystalline region of the polymers followed by the formation of a dynamic balanced new interfacial region.^{16,40} The addition of nanocellulose facilitated the shift from multiple phases to a homogeneous phase through the attraction of PVA and PEO chains as interfacial compatibilizers.

CONCLUSIONS

CNCs and CNFs were used as interfacial compatibilizers in PVA and PEO blend nanocomposites by a solution casting method. Their effects on the morphologies, mechanical properties, thermal properties, and crystalline structures of the nanocomposites were systematically studied. We found that the nanocellulose was more highly efficient at improving the interfacial miscibility of the polymer blends rather than strengthening a single polymer. The mechanical reinforcement was mainly attributed to the hydrogen bonding with PVA and PEO and led to parts of the crystalline region reorganizing successfully around the interface. CNCs led to a higher strength, modulus, and better thermal stability than CNFs did at the same content because of their good dispersion and smaller aspect ratio. The lesser entanglement of the CNCs resulted in more chances for them to interact with the matrix and break down parts of the crystalline region. CNCs also offered more help in shifting the polymer blends from separated phases to a homogeneous phase. The results of simulations of two models were compared with the experimental results, and this comparison reinforced the assumption that the effect of the strengthened interfacial miscibility had a prominent role. The unique function offered by the CNCs and CNFs provided a fundamental and comparative insight into the selection of nanocellulose materials as interfacial compatibilizers.

ACKNOWLEDGMENTS

This work was financially supported by the National State Bureau of Forestry 948 Plan of China (contract grant number 2014-4-49), the Priority Academic Program Development of Jiangsu Higher Education Institutions, the Doctorate Fellowship Foundation of Nanjing Forestry University, and Scientific Innovation Research of College Graduates in Jiangsu Province (contract grant number KYZZ-0251).

REFERENCES

- Mao, H.; Zhang, T.; Zhang, N.; Huang, T.; Yang, J.; Wang, Y. *Polym. Int.* **2016**, *65*, 1417.
- Yang, J.-H.; Feng, C.-X.; Chen, H.-M.; Zhang, N.; Huang, T.; Wang, Y. *Polym. Int.* **2016**, *65*, 675.
- Ramya, P.; Ranganathaiah, C.; Williams, J. F. *Polymer* **2012**, *53*, 4539.
- Wu, D.; Yuan, L.; Laredo, E.; Zhang, M.; Zhou, W. *Ind. Eng. Chem. Res.* **2012**, *51*, 2290.
- Li, L.; Chen, N.; Wang, Q. *J. Polym. Sci. Part B: Polym. Phys.* **2010**, *48*, 1946.
- Li, Y.; Wu, W.; Lin, F.; Xiang, A. *J. Appl. Polym. Sci.* **2012**, *126*, 162.
- Mishra, R.; Rao, K. *J. Eur. Polym. J.* **1999**, *35*, 1883.
- Lai, W. C.; Liao, W. B. *J. Appl. Polym. Sci.* **2004**, *92*, 1562.
- Sawatari, C.; Kondo, T. *Macromolecules* **1999**, *32*, 1949.
- Agarwal, R.; Alam, M. S.; Gupta, B. *J. Appl. Polym. Sci.* **2013**, *129*, 3728.
- Gupta, B.; Agarwal, R.; Alam, M. S. *J. Appl. Polym. Sci.* **2013**, *127*, 1301.
- Javadi, A.; Zheng, Q.; Payen, F.; Altin, Y.; Cai, Z.; Sabo, R.; Gong, S. *ACS Appl. Mater. Interfaces* **2013**, *5*, 5969.
- Xu, X.; Wang, H.; Jiang, L.; Wang, X.; Payne, S. A.; Zhu, J. Y.; Li, R. *Macromolecules* **2014**, *47*, 3409.

14. Xu, X.; Liu, F.; Jiang, L.; Zhu, J. Y.; Haagenson, D.; Wiesenborn, D. P. *ACS Appl. Mater. Interfaces* **2013**, *5*, 2999.
15. Siqueira, G.; Bras, J.; Dufresne, A. *Biomacromolecules* **2009**, *10*, 425.
16. Estridge, C. E.; Jayaraman, A. *ACS Macro Lett.* **2015**, *4*, 155.
17. Sun, X.; Wu, Q.; Ren, S.; Lei, T. *Cellulose* **2015**, *22*, 1123.
18. Oun, A. A.; Rhim, J.-W. *Mater. Lett.* **2016**, *168*, 146.
19. Ben Azouz, K.; Ramires, E. C.; Van den Fonteyne, W.; El Kissi, N.; Dufresne, A. *ACS Macro Lett.* **2012**, *1*, 236.
20. Abd El-Kader, F. H.; Hakeem, N. A.; Elashmawi, I. S.; Ismail, A. M. *Indian J. Phys.* **2013**, *87*, 983.
21. Saklar, S.; Yorukoglu, A. *Physicochem. Probl. Miner. Process.* **2015**, *51*, 83.
22. Liu, A.; Walther, A.; Ikkala, O.; Belova, L.; Berglund, L. A. *Biomacromolecules* **2011**, *12*, 633.
23. Zhang, Z.; Wang, S.; Zhang, J. *Polym. Compos.* **2014**, *35*, 2365.
24. Fortunati, E.; Puglia, D.; Luzi, F.; Santulli, C.; Kenny, J. M.; Torre, L. *Carbohydr. Polym.* **2013**, *97*, 825.
25. Khoshkava, V.; Kamal, M. R. *ACS Appl. Mater. Interfaces* **2014**, *6*, 8146.
26. Van Es, M. A.; Xiqiao, F.; Van Turnhout, J.; Van der Giessen, E. In *Speciality Polymer Additives: Principles and Applications*; Al-Malaika, S., Golovoy, A., Wilkie, C. A., Eds.; Wiley-Blackwell: New York, **2001**; p 391.
27. Sturcova, A.; Davies, G. R.; Eichhorn, S. J. *Biomacromolecules* **2005**, *6*, 1055.
28. Cox, H. L. Br. *J. Appl. Phys.* **1952**, *3*, 72.
29. Ouali, N.; Cavaille, J. Y.; Perez, J. *Plast. Rubber Compos. Process. Appl.* **1991**, *16*, 55.
30. Takayanagi, M.; Uemura, S.; Minami, S. *J. Polym. Sci. Part C: Polym. Symp.* **1964**, *5*, 113.
31. Favier, V.; Chanzy, H.; Cavaille, J. Y. *Macromolecules* **1995**, *28*, 6365.
32. Sirvio, J. A.; Honkaniemi, S.; Visanko, M.; Liimatainen, H. *ACS Appl. Mater. Interfaces* **2015**, *7*, 19691.
33. Aloui, H.; Khwaldia, K.; Hamdi, M.; Fortunati, E.; Kenny, J. M.; Buonocore, G. G.; Lavorgna, M. *ACS Sustain. Chem. Eng.* **2016**, *4*, 794.
34. de Sainte Claire, P. *Macromolecules* **2009**, *42*, 3469.
35. Jakić, M.; Vrandečić, N. S.; Klarić, I. *Polym. Degrad. Stab.* **2013**, *98*, 1738.
36. Peng, Y.; Gardner, D. J.; Han, Y. *Cellulose* **2015**, *22*, 3199.
37. Roma, M.; Winter, W. T. *Biomacromolecules* **2004**, *5*, 1671.
38. Dufresne, A.; Kellerhals, M. B.; Witholt, B. *Macromolecules* **1999**, *32*, 7396.
39. Wunderlich, B.; Pyda, M.; Pak, J.; Androsch, R. *Thermochim. Acta* **2001**, *377*, 9.
40. Gödel, A.; Marmur, A.; Kasaliwal, G. R.; Pötschke, P.; Heinrich, G. *Macromolecules* **2011**, *44*, 6094.